Relationship between sensitivity and waveguide position on the diaphragm in integrated optic pressure sensors based on the elasto-optic effect

Masashi Ohkawa, Kazuhiko Hasebe, Seishi Sekine, and Takashi Sato

The sensitivities of integrated optic pressure sensors with diaphragms theoretically are known to be strongly dependent on the position of the sensing waveguide on the diaphragm. According to the theoretical results, the diaphragm edge is the best position for the waveguide of a sensor based on the elasto-optic effect. The relationship between sensitivity and the waveguide position, however, has not been investigated experimentally, although it is important in the designing of such a sensor and in determining the misalignment tolerance of the sensing waveguide. In this study, this relationship in a glass-based integrated optic sensor by use of an intermodal interference was examined experimentally.

OCIS codes: 060.2370, 120.3180, 130.3120, 130.6010, 230.3120, 130.0130.

1. Introduction

Since the late 1980s, integrated optic sensors incorporated with micromechanical structures have been attracting much attention owing to the remarkable development of silicon micromachining technologies.[1] Several groups demonstrated interferometric pressure sensors with micromachined diaphragms as pressure-sensitive structures.[2-8] Regarding these sensors, it is known theoretically that sensitivity is strongly dependent on the position of the sensing waveguide over the diaphragm. According to the theoretical prediction, the sensing waveguide should be placed along a diaphragm edge in the sensors based on the elasto-optic effect.[2,6] However, it was not experimentally known how sensitivity is related to the waveguide position. The experimental investigation of their dependence is very significant to the design of a sensor with higher sensitivity and to the consideration of the misalignment tolerance of the waveguide position. In this study, their relationship was examined experimentally with a sensor based on intermodal interference between the fundamental TM-like and TE-like modes in a single-mode waveguide. Since this type of sensor requires only a straight waveguide, many waveguides, or inteferometers, can be spaced closely to each other on a diaphragm to determine the relationship between sensitivity and waveguide position. If, however, the conventional Mach–Zehnder interferometer were used, many sensing waveguides could not be placed with minimal separation on the diaphragm, since the interferometer requires the reference waveguide to be separated sufficiently from the diaphragm and the sensing waveguide. Furthermore, a glass substrate was utilized to build the sensor, although silicon is the more familiar substrate for sensors incorporated with mechanical structures. The use of a glass substrate brings a reliable comparison between the theoretical and the experimental results, because its mechanical and optical parameters are well known. The results obtained in this study could be modified for any interferometric pressure sensor based on the elasto-optic effect.

2. Integrated Optic Pressure Sensor with Use of Intermodal Interference

Figure 1 shows an integrated optic pressure sensor designed for this study. The sensor is composed of a diaphragm as a pressure-sensitive mechanical structure and closely spaced single-mode waveguides over the diaphragm. The waveguides hold the funda-

At the time of this research, the authors were with the Faculty of Engineering, Niigata University, 8050 Ikarashi 2-no-cho, Niigata 950-2181, Japan. K. Hasebe is now with Matsushita Communication Sendai Research and Development Laboratories Company, Ltd., Sendai 981-3206, Japan. M. Ohkawa's email address is ohkawa@eng.niigata-u.ac.jp.

Received 28 September 2001; revised manuscript received 29 April 2002.
0003-6935/02/245016-06$15.00/0

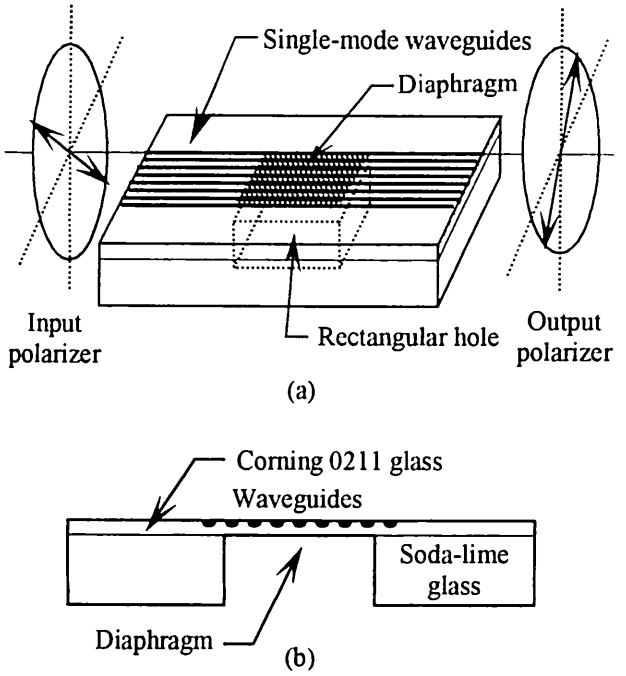

Fig. 1. (a) Schematic drawing of the integrated optic pressure sensor placed between a pair of crossed polarizers and (b) its cross sectional view. The sensor has 24 waveguides on the diaphragm to determine the relationship between phase sensitivity and waveguide position.

mental TM-like and TE-like modes that are associated with the intermodal interference. The diaphragm is distorted when a pressure difference is applied to it. The distortion causes strain, which in turn produces a change in the refractive index of the diaphragm through the elasto-optic effect. The index change yields phase retardation in the lightwave, which is propagated in the waveguides across the diaphragm. Since the phase retardation is dependent on the guided modes, the phase difference between the TM-like and TE-like modes varies as a function of the applied pressure difference. The phase difference between the two modes can be transferred into lightwave intensity by a pair of crossed polarizers. The sensor is placed between two polarizers, as shown in Fig. 1(a). The input polarizer is oriented at 45° with respect to the polarization of each guided mode. The light beam through the input polarizer is coupled to the TM-like and TE-like modes at equal intensities. At the end of the waveguides, the lightwave has linear, elliptic, or circular polarization, corresponding to the induced phase difference between the two guided modes. The crossed output polarizer converts the polarization-modulated light into intensity-modulated light.

3. Theoretical Analysis

A. Mathematical Description

In the analysis, a rectangular plate with an area of $a \times b$ and a thickness of t is assumed as the diaphragm, shown in Fig. 2. The y–z plane lies on the middle plane between both surfaces of the diaphragm, and the z axis is parallel to the waveguide. The x axis is perpendicular to the plate surface. The diaphragm is also assumed to be isotropic mechanically and optically. The deflection w of the diaphragm, or displacement from the equilibrium position, due to the uniformly applied pressure q is obtained from the following differential equation:

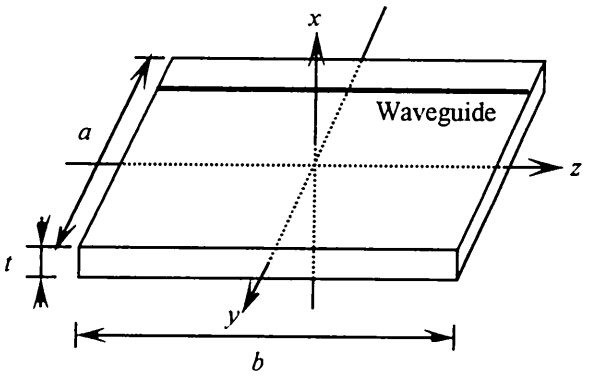

Fig. 2. Illustration of the rectangular diaphragm assumed in the calculations.

$$\frac{\partial^4 w}{\partial y^4} + 2\frac{\partial^4 w}{\partial y^2 \partial z^2} + \frac{\partial^4 w}{\partial z^4} = \frac{q}{D}. \tag{1}$$

D is flexural rigidity defined as $D = Yt^3/12(1 - \rho^2)$.[9] Y and ρ denote the modulus of elasticity and the Poisson's ratio, respectively. When all edges are rigidly clamped, the solution to Eq. (1) is given in a sum form as follows:

$$w = w_0 + w_1 + w_2, \tag{2}$$

$$w_0 = \frac{4qa^4}{\pi^5 D} \sum_{m=1,3,5,\ldots}^{\infty} \frac{(-1)^{(m-1)/2}}{m^5} \times \left(1 - \frac{\alpha_m \tanh \alpha_m + 2}{2 \cosh \alpha_m} \cosh \frac{m\pi z}{a} + \frac{1}{2 \cosh \alpha_m} \frac{m\pi z}{a} \sinh \frac{m\pi z}{a}\right) \cos \frac{m\pi y}{a}, \tag{3}$$

$$w_1 = -\frac{a^2}{2\pi^2 D} \sum_{m=1,3,5,\ldots}^{\infty} E_m \frac{(-1)^{(m-1)/2}}{m^2 \cosh \alpha_m} \times \left(\frac{m\pi z}{a} \sinh \frac{m\pi z}{a} - \alpha_m \tanh \alpha_m \cosh \frac{m\pi z}{a}\right) \cos \frac{m\pi y}{a}, \tag{4}$$

$$w_2 = -\frac{b^2}{2\pi^2 D} \sum_{m=1,3,5,\ldots}^{\infty} F_m \frac{(-1)^{(m-1)/2}}{m^2 \cosh \beta_m} \times \left(\frac{m\pi y}{b} \sinh \frac{m\pi y}{b} - \beta_m \tanh \beta_m \cosh \frac{m\pi y}{b}\right) \cos \frac{m\pi z}{b}, \tag{5}$$

where $\alpha_m = m\pi b/2a$ and $\beta_m = m\pi a/2b$.[9] E_m and F_m in Eqs. (4) and (5) are determined to satisfy the following boundary conditions:

$$\left(\frac{\partial w_0}{\partial z}\right)_{z=b/2} + \left(\frac{\partial w_1}{\partial z} + \frac{\partial w_2}{\partial z}\right)_{z=b/2} = 0, \tag{6}$$

$$\left(\frac{\partial w_0}{\partial y}\right)_{y=a/2} + \left(\frac{\partial w_1}{\partial y} + \frac{\partial w_2}{\partial y}\right)_{y=a/2} = 0. \tag{7}$$

From the solved deflection, the normal stresses σ_x, σ_y, and σ_z are calculated according to the following equations:

$$\sigma_x = T_1 = -\frac{3q}{4}\left[\frac{2}{3} - \frac{2}{t}x + \frac{1}{3}\left(\frac{2}{t}x\right)^3\right], \tag{8}$$

$$\sigma_y = T_2 = -\frac{Yx}{1-\rho^2}\left(\frac{\partial^2 w}{\partial y^2} + \rho\frac{\partial^2 w}{\partial z^2}\right), \tag{9}$$

$$\sigma_z = T_3 = -\frac{Yx}{1-\rho^2}\left(\frac{\partial^2 w}{\partial z^2} + \rho\frac{\partial^2 w}{\partial y^2}\right). \tag{10}$$

The stress has six components, which are divided into two types: normal stress and shearing stress ($\tau_{yz} = \tau_{zy} = T_4$, $\tau_{zx} = \tau_{xz} = T_5$, $\tau_{xy} = \tau_{yx} = T_6$). Shearing stress can be neglected under the condition that the deflection is small in comparison with the thickness of the diaphragm. When the stress T and strain S obey Hooke's law, their relationship is written as

$$S_i = s_{ij}T_j \qquad (i, j = 1,\ldots, 6), \tag{11}$$

where the tensor s_{ij} denotes the mechanical compliance. The anisotropic index change Δn_i caused by the strain is given by the following equation, including the elasto-optic coefficient p_{ij}:

$$\Delta n_i = -\frac{1}{2}n^3 p_{ij}S_j \qquad (i, j = 1,\ldots, 6), \tag{12}$$

where n is the refractive index of the diaphragm. The change in the refractive index causes phase retardation to the lightwave traveling on the diaphragm. Phase retardations for the TM-like and TE-like modes are expressed simply under the scalar field approximation as

$$\Delta\phi_{TM} \approx \int_{-b/2}^{b/2}\left[\frac{\omega\varepsilon_0 n}{2}\int_{-a/2}^{a/2}\int_{-t/2}^{t/2} E_x(x, y) \times \Delta n_1(x, y, z)E_x^*(x, y)\mathrm{d}x\mathrm{d}y\right]\mathrm{d}z, \tag{13}$$

$$\Delta\phi_{TE} = \int_{-b/2}^{b/2}\left[\frac{\omega\varepsilon_0 n}{2}\int_{-a/2}^{a/2}\int_{-t/2}^{t/2} E_y(x, y) \times \Delta n_2(x, y, z)E_y^*(x, y)\mathrm{d}x\mathrm{d}y\right]\mathrm{d}z, \tag{14}$$

where ω is the angular frequency of the light, ε_0 is the permittivity of the vacuum, and * indicates the complex conjugate. Also, E_x and E_y are the power-normalized x-directed electric field component of the TM-like mode and the y-directed electric field component of the TE-like mode, respectively. The expression in the brackets for each equation represents the local phase retardation per unit length, which is finally integrated with respect to z to obtain the total retardation. In the sensor that uses the intermodal interference, the contributing phase change $\Delta\phi$ is the difference between the phase retardations of the TM-like and TE-like modes, and is therefore given by

$$\Delta\phi = \Delta\phi_{TM} - \Delta\phi_{TE}. \tag{15}$$

The phase sensitivity, defined as the resultant phase difference per unit pressure, is used for the evaluation in this study. In the calculation, the phase retardation due to elongation of the waveguide by deformation is neglected, because the deflection is assumed to be significantly smaller than the diaphragm thickness.

B. Calculated Sensitivity versus Waveguide Position

The induced index change is not distributed uniformly in the diaphragm, so that the induced phase difference per unit pressure (the phase sensitivity) is dependent on the position of the waveguide over the diaphragm. The phase sensitivity was calculated as a function of the waveguide position, following the above mathematical description. In the calculation, the pressure was assumed to be applied uniformly over the diaphragm with all the edges clamped. Numerical results were computed with the mechanical and optical parameters of the Corning 0211 glass, except for the elasto-optic coefficients of fused silica. These parameters used are described in Appendix A. In addition, it was assumed that the waveguide had a step-index rectangular profile in order to simplify the calculations of the electric fields of the guided modes. If the guided waves are well confined, the index profile does not affect notably the calculated results. Figure 3 shows the calculated sensitivity versus the waveguide position. In the figure, the length–width ratio of the diaphragm is taken as a parameter. The normalized waveguide position is defined as the waveguide position in the y direction divided by the width a of the diaphragm. The center of the diaphragm corresponds to 0, and the diaphragm edges to ± 0.5. The calculated sensitivity is normalized to be at unity at the diaphragm edges in the y direction for each ratio. It is found from Fig. 3 that the sensitivity takes the maximum value when

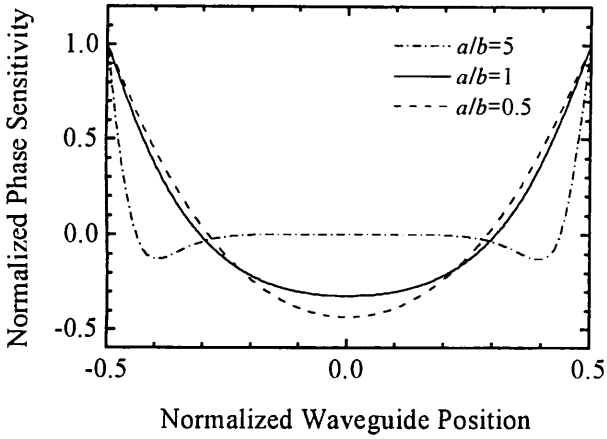

Fig. 3. Relationships between normalized sensitivity and waveguide position in the y direction. Normalized waveguide positions of ± 0.5 indicate that the waveguide is placed along the diaphragm edge, whereas a position of 0 corresponds to the center of the diaphragm.

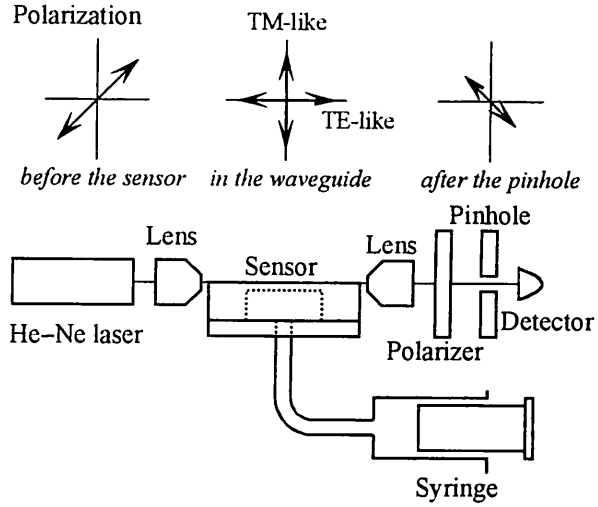

Fig. 4. Experimental setup to measure the output intensity as a function of the applied pressure.

the waveguide is located along the edge for any ratio. In other words, to maximize the sensitivity of the sensor, the diaphragm edge is the best waveguide position. Moreover, the sensitivities at the edge and at the center have opposite signs, and there is a position where the sensitivity becomes zero between the edge and the center. For the square diaphragm, the calculated sensitivity at edge is two-thirds times greater than that at center.

4. Experiments

A. Fabrication

The fabricated sensor had 24 straight waveguides spaced at 0.5-mm intervals to determine the dependence of the sensitivity on the waveguide position on the diaphragm. The sensor was built with two glass substrates: a 0.3-mm-thick substrate for waveguide formation and a 1.8-mm-thick substrate with a 10 mm $\times$ 10 mm square hole as a support structure of the diaphragm. Since the square hole determined the diaphragm area, the length and width of the diaphragm were 10 mm each, and the ratio between them was 1. First, a thin aluminum film was evaporated on a Corning 0211 glass substrate 0.3 mm thick. On the aluminum film, the waveguide pattern with a width of about 5 μm was engraved by a photolithographic process. Then, the glass with the patterned aluminum film as a mask was immersed in pure KNO_3 for two hours at 400 °C to form single-mode channel waveguides by the potassium-ion exchange. Before the two substrates were put together, one of the waveguides was aligned above a side of the hole in the thick glass substrate. Finally, both substrates were bonded together by UV adhesion.

B. Results and Discussions

Figure 4 shows the experimental setup. The fabricated sensor was tested with a linearly polarized He–Ne laser at 633 nm. The polarization of the laser beam was set at 45° to the sensor surface, so that the input polarizer shown in Fig. 1(a) was not necessary in this experiment. The output light from the sensor was passed through a pinhole, blocking most stray light. To apply pressure to the diaphragm, a syringe was connected to the sensor by a silicone tube. We applied the pressure difference, ranging from -60 to $+85$ kPa, to the diaphragm by pulling and pushing the plunger of the syringe, and determined this difference from the ideal gas law. A positive value represents a pressure in the hole that is higher than the atmospheric pressure. Figures 5(a)–5(e) show the normalized output intensity as a function of the applied pressure for the waveguides placed at 0.35, 1.35, 2.35, 3.35, and 4.35 mm from the center of the diaphragm, respectively. The normalized intensity was defined as the measured output intensity divided by the expected maximum intensity. The solid curve in each figure indicates the computer projection of the measured data. From the sinusoidal curves in Figs. 5(a)–(e), the half-wave pressures are evaluated to be 127, 202, 241, 433, and 113 kPa, corresponding to the sensitivities of 24.7, 15.6, 13.0, 7.3, and 27.9 mrad/kPa, respectively. Extinction ratios were low, since the stray light was not completely blocked by the pinhole. The same measurement was also taken for the other waveguides. Figure 6 indicates the measured sensitivity for each waveguide and the theoretical curve. The experimental results agree with the theoretical curve, although there is a large difference near the diaphragm edge. The measured sensitivity took the maximum value for the nearest waveguide to the diaphragm edge as predicted from the theoretical analysis, but it was almost half the calculated sensitivity. It is presumed that this undesirable reduction of the sensitivity was caused by the relaxation of the induced strain near the diaphragm edge. To indicate the existence of strain relaxation, we mea-

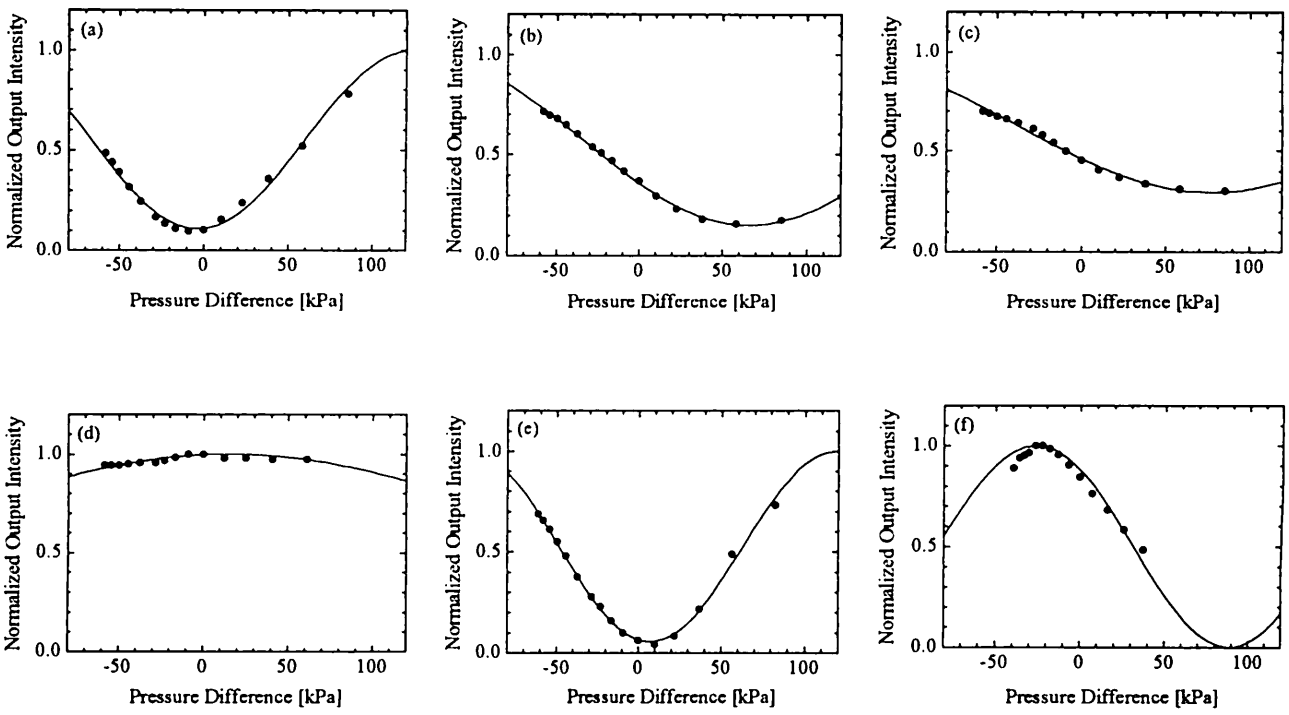

Fig. 5. These figures indicate the experimental results of normalized output intensity versus applied pressure difference for waveguides placed at (a) 0.35, (b) 1.35, (c) 2.35, (d) 3.35, and (e) 4.35 mm from the center of the diaphragm. Also, (f) is for a waveguide located 0.35 mm outside of the diaphragm edge.

sured the output intensity versus the applied pressure for the waveguide placed at 0.35 mm outside the diaphragm edge. Figure 5(f) shows the experimental result. The output intensity seems to change sinusoidally with the applied pressure. Its half-wave pressure is evaluated to be 115 kPa, corresponding to a sensitivity of 27.3 mrad/kPa, from the best-fit sinusoidal curve in the ideal case of the infinite extinction ratio. Since the ratio is finite, the sensitivity is a little higher than 27.3 mrad/kPa. The relatively large sensitivity was observed even for the waveguide position outside the diaphragm. The result suggests that the strained region exists beyond the diaphragm and that the strain relaxes around the diaphragm edge. Such relaxation was caused mainly by the imperfect bonding by UV adhesion, which reduced rigidity of the support structure surrounding the diaphragm. If the support structure were made more rigid, the measured sensitivity for the waveguide position near the diaphragm edge would be improved.

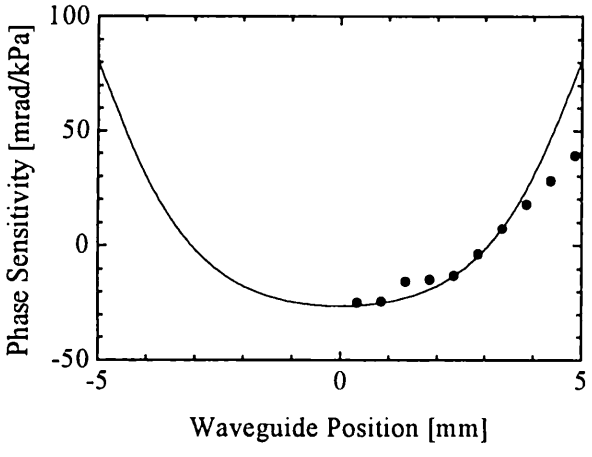

Fig. 6. Measured phase sensitivity as a function of the waveguide position on the diaphragm.

5. Conclusions

We experimentally determined the relationship between sensitivity and waveguide position on the diaphragm. The measured sensitivities agreed well with the calculated sensitivities for all waveguide positions except near the edge. The measured and theoretical results show that the diaphragm edge is the best position regarding sensitivity. Regarding the misalignment tolerance of the waveguide position, the center position is better than the edge. If one emphasizes misalignment tolerance of the waveguide, which becomes severe in diaphragms of narrow width, the center waveguide position is preferred. In this study, the measured sensitivity at the center was almost the same as that at the edge because of the undesirable reduction of the sensitivity near the edge. The reduction was attributed mainly to the imperfect bonding of the two glass substrates. To rectify the cause, the diaphragm edge should be clamped rigidly in order to increase the sensitivity close to the theoretical estimation. This cause is not, however, significant for a sensor using a silicon diaphragm, because bonding is not necessary.

Appendix A

In the numerical calculations, we used the mechanical and optical parameters of the Corning 0211 glass, of which the diaphragm was made, except for the elasto-optic coefficients of the fused silica. The use of the elasto-optic coefficients of the fused silica would not affect greatly the numerical result, because silica is the principal ingredient of the Corning 0211 glass. The refractive index n of the diaphragm, the modulus of elasticity Y, Poisson's ratio ρ, the compliance s_{ij} and the elasto-optic coefficients p_{ij} were as follows:

$$n = 1.523, \qquad Y = 7.44 \times 10^{10}\ \text{Pa}, \qquad \rho = 0.22,$$

$$s_{ij} = \begin{pmatrix} s_{11} & s_{12} & s_{12} & 0 & 0 & 0 \\ s_{12} & s_{11} & s_{12} & 0 & 0 & 0 \\ s_{12} & s_{12} & s_{11} & 0 & 0 & 0 \\ 0 & 0 & 0 & s_{44} & 0 & 0 \\ 0 & 0 & 0 & 0 & s_{44} & 0 \\ 0 & 0 & 0 & 0 & 0 & s_{44} \end{pmatrix},$$

$$s_{11} = 1.37 \times 10^{-11}\ \text{Pa}^{-1},$$

$$s_{12} = -2.33 \times 10^{-12}\ \text{Pa}^{-1},$$

$$s_{44} = 3.20 \times 10^{-11}\ \text{Pa}^{-1},$$

$$p_{ij} = \begin{pmatrix} p_{11} & p_{12} & p_{12} & 0 & 0 & 0 \\ p_{12} & p_{11} & p_{12} & 0 & 0 & 0 \\ p_{12} & p_{12} & p_{11} & 0 & 0 & 0 \\ 0 & 0 & 0 & p_{44} & 0 & 0 \\ 0 & 0 & 0 & 0 & p_{44} & 0 \\ 0 & 0 & 0 & 0 & 0 & p_{44} \end{pmatrix},$$

$$p_{11} = 1.21 \times 10^{-1},$$

$$p_{12} = 2.70 \times 10^{-1},$$

$$p_{44} = 7.45 \times 10^{-2}.$$

This work is, in part, supported by a Grant-in-Aid for Scientific Research (No. 12650339) from the Japan Society for the Promotion of Science.

References

1. M. Tabib-Azar and G. Beheim, "Modern trends in microstructures and integrated optics for communication, sensing, and actuation," Opt. Eng. **36,** 1307–1318 (1997).
2. M. Ohkawa, M. Izutsu, and T. Sueta, "Integrated optic pressure sensor on silicon substrate," Appl. Opt. **28,** 5153–5157 (1989).
3. G. N. De Brabander, G. Beheim, and J. T. Boyd, "Integrated optical micromachined pressure sensor with spectrally encoded output and temperature compensation," Appl. Opt. **37,** 3264–3267 (1998).
4. H. Porte, V. Gorel, S. Kiryenko, J. Goedgebuer, W. Daniau, and P. Blind, "Imbalanced Mach–Zehnder interferometer integrated in micromachined silicon substrate for pressure sensor," J. Lightwave Technol. **17,** 229–233 (1999).
5. G. N. De Brabander, J. T. Boyd, and G. Beheim, "Integrated optical ring resonator with micromechanical diaphragm for pressure sensing," IEEE Photon. Technol. Lett. **6,** 671–673 (1994).
6. M. Ohkawa, K. Hasebe, C. Nishiwaki, S. Sekine, and T. Sato, "Integrated optical pressure sensor using intermodal interference between two mutual orthogonal guided-modes," Opt. Rev. **7,** 144–148 (2000).
7. Y. Shirai, T. Goto, M. Ohkawa, S. Sekine, and T. Sato, "Silicon-based integrated optical pressure sensor using intermodal interference between TM-like and TE-like modes," in *Integrated Optic Devices V*, G. C. Righini and S. Honkanen, eds., Proc. SPIE **4277,** 411–418 (2001).
8. A. Yamada, Y. Shirai, T. Goto, M. Ohkawa, S. Sekine, and T. Sato, "Relationship between sensitivity and waveguide position on diaphragm for silicon-based integrated optic pressure sensor," in *Technical Digest Volume I of 4th Pacific Rim Conference on Lasers and Electro-Optics* (Institute of Electrical and Electronics Engineers, New York, 2001), pp. 420–421.
9. S. P. Timoshenko and S. Woinowsky-Krieger, *Theory of Plates and Shells* (McGraw-Hill Kogakusha, Tokyo, 1981).